Inorganic Chemistry

Article

pubs.acs.org/IC

Cyanide-Bridged $W^{V}Mn^{III}$ Bimetallic Chains Composed of a Blocked W Hexacyanide Precursor: Geometry-Related Magnetic Couplings and Magnetostructural Correlation

Jin Wuk Lee,[†] Kwang Soo Lim,[†] Dae Won Ryu,[†] Eui Kwan Koh,[‡] Sung Won Yoon,[§] Byoung Jin Suh,[§] and Chang Seop Hong*[,†]

[†]Department of Chemistry, Research Institute for Natural Sciences, Korea University, Seoul 136-713, Korea

[‡]Nano-Bio System Research Team, Korea Basic Science Institute, Seoul 136-713, Korea

[§]Department of Physics, The Catholic University of Korea, Buchon 420-743, Korea

Supporting Information

ABSTRACT: Five one-dimensional bimetallic $W^{V}Mn^{III}$ complexes **1**−**5**, consisting of $[W(CN)_6(bpy)]^-$ anions and $[Mn(Schiff\ base)]^+$ cations, were prepared. The central coordination geometry around each W atom is determined as a distorted dodecahedron (DD) for **1** and **2**, and a distorted square antiprism (SAPR) for **3**−**5**. Magnetic analyses demonstrate that compounds **1**, **4**, and **5** exhibit antiferromagnetic interactions between magnetic centers, which are different from the ferromagnetic couplings in **2** and **3**. For the distorted DD geometry, the Mn−N_{ax} (ax = axial) bond length increases when moving from **1** to **2**, with the Mn−N_{ax}−C_{ax} angle remaining constant. The elongation of the bond length is responsible for the reduction in orbital overlap and consequent ferromagnetic coupling in **2**. In comparison, for **3**−**5** with the distorted SAPR geometry, given that the Mn−N_{ax} bond lengths are similar across all the samples, the increase in the Mn−N_{ax}−C_{ax} angles accounts for the enhanced magnetic strength. Notably, a correlation between structure and magnetic exchange coupling is established for the first time in $W^{V}Mn^{III}$ bimetallic systems based on the $[W(CN)_6(bpy)]^-$ precursor.

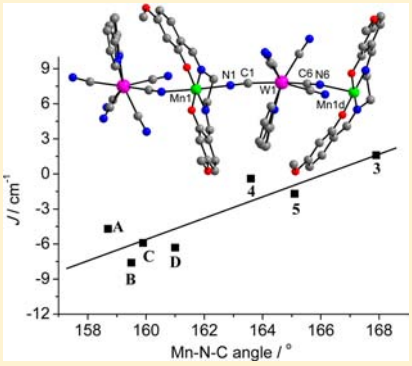

INTRODUCTION

Molecule-based magnetic materials have been explored intensively because of their fundamental interest and potential applications in magnetic devices.[1−4] One of the merits of molecular magnetic materials is that specific magnetic traits in the molecular solids can be inserted intentionally by utilizing the emergent intrinsic properties of compositional metal centers and ligands with various functionalities.[5,6] The aforementioned advantages provide plenty of intriguing characteristics in molecular assemblies such as anisotropy-related magnetism, chirality, magnetization-induced second harmonic generation, photomagnetism, and so on.[7,8]

Compared with 3d-based magnetic systems, magnetic assemblies with enhanced exchange couplings and anisotropic properties can be constructed with 4d/5d metal ions, because they possess more radially extended orbitals and exhibit greater spin−orbit coupling. From the viewpoint of coordination chemistry, 4d/5d-transition-metal complexes provide greater stability for higher oxidation states and coordination numbers above six. The design strategy for attaining such molecular magnetic systems involves the use of building blocks with second coordination sites that bind neighboring spin centers. Although there are many other types of useful building units with appropriate ligands, molecular precursors equipped with cyanide ligands constitute the majority of known 4d/5d magnetic materials.[8] Cyanide-linked building blocks can be classified into two groups: (i) the first group is based on a metal ion surrounded by cyanide groups only, for instance, $M(CN)_p^{q-}$ (M = 4d/5d metal ions, p = 6−8), and (ii) the second group includes metal cyanides decorated with blocking ligands that can restrict molecular dimensionality.[7−11] Cyanometallates, $M(CN)_p^{q-}$, can be successfully implemented in assembled systems with structures ranging from discrete molecules to high-dimensional networks.[7] The dimensionality is controlled by introducing metal counterparts with limited available coordination sites into the assembly process together with the cyanometallate building bricks. On the other hand, metal cyanides capped with blocking groups are frequently utilized to generate low-dimensional systems, since the capping ligands prevent the expansion of molecular structures to higher dimensionalities.[12,13] In particular, the precursors serve as efficient synthons for the formation of single-molecule magnets (SMMs) and single-chain magnets (SCMs) when magnetic anisotropy is properly incorporated into the low-dimensional systems.[14−16]

The elucidation of the magnetic exchange coupling mechanism provides essential information on the magnetic

Received: April 5, 2013
Published: July 16, 2013

   dx.doi.org/10.1021/ic400845z | Inorg. Chem. 2013, 52, 8677−8684

Table 1. Crystallographic Data for 1−5

	1	2	3	4·1.5H_2O	5·2H_2O
formula	$C_{36}H_{30}MnN_{10}O_4W$	$C_{37}H_{32}MnN_{10}O_4W$	$C_{38}H_{32}MnN_{10}O_4W$	$C_{68}H_{58}Mn_2N_{20}O_{11}W_2$	$C_{35}H_{32}MnN_{10}O_6W$
M_r	905.49	919.52	931.53	1808.92	927.50
T (K)	296(2)	296(2)	130(2)	296(2)	293(2)
crystal system	monoclinic	monoclinic	orthorhombic	orthorhombic	orthorhombic
space group	$P2_1/n$	$P2_1/n$	$Pbca$	$Pbcn$	$Pbcn$
a (Å)	9.2490(2)	9.2036(2)	9.1591(6)	34.516(5)	35.34(3)
b (Å)	20.7220(4)	21.1875(5)	21.9836(12)	9.1596(14)	9.224(9)
c (Å)	18.0289(3)	18.0645(4)	36.153(2)	21.727(4)	21.82(2)
α (deg)	90	90	90	90	90
β (deg)	92.4420(10)	92.8530(10)	90	90	90
γ (deg)	90	90	90	90	90
V (Å^3)	3452.24(12)	3518.23(14)	7279.5(8)	6868.8(18)	7112(12)
Z	4	4	8	4	8
ρ_{calc} (g cm^{-3})	1.742	1.736	1.700	1.749	1.732
μ (mm^{-1})	3.752	3.683	3.561	3.774	3.648
F(000)	1788	1820	3688	3568	3672
GOF	1.010	0.866	1.051	0.980	1.016
R1[a] ($I \geq 2\sigma(I)$)	0.0372	0.0464	0.1012	0.0461	0.0689
wR2[b] ($I \geq 2\sigma(I)$)	0.0736	0.0629	0.1355	0.0724	0.1461

[a] $R1 = \sum||F_o| - |F_c||/\sum|F_o|$. [b] $wR2 = [\sum[w(F_o^2 - F_c^2)^2]/\sum[w(F_o^2)^2]]^{1/2}$.

phenomena of molecular systems. Material design in pursuit of desirable magnetic properties refers to the magnetic exchange coupling occurring between adjacent spin centers, since the magnetic features are obviously dictated by magnetic coupling. A series of $M'^{III}Mn^{III}$ bimetallic compounds (M' = Fe, Cr) composed of paramagnetic metal cyanides and anisotropic Mn^{III} Schiff bases were studied, and their magnetostructural correlations were investigated.[17−22] For cyanide-bridged $Fe^{III}Mn^{III}$ complexes, the magnetic properties are altered according to the change in their Mn−N_{ax}−C_{ax} (ax = axial) angles, which arise from competing overlaps between relevant magnetic orbitals.[12] Interestingly, the trend of the coupling constant (J) is dependent on the Fe^{III} tricyanides used. Although the delicate contributions from the Mn−N bond lengths and Mn−N−C−Fe torsion angles in the bridging pathways cannot be ruled out in the variation of the coupling constant, the J value in *facial* Fe tricyanide-linked $Fe^{III}Mn^{III}$ systems is prone to decrease as the angle increases,[19] while the opposite tendency of J is observed in bimetallic assemblies formed by *meridional* Fe tricyanides.[21] Hence, it is important to corroborate the respective exchange mechanism that is sensitive to the individual magnetic systems of interest. Numerous examples of 4d/5d-based bimetallic systems have been reported so far, displaying a variety of fascinating features.[7,8] The magnetic strengths in octacyanotungstate-based bimetallic complexes were suggested to be regulated by the local geometry around the W center.[23,24] However, systematic studies on the fundamental structure−property relationships are still scarce in 4d/5d-transition-metal-based materials, and therefore need to be thoroughly investigated for a better understanding of magnetic properties of such materials.[7,25−28]

Herein, we report the syntheses, crystal structures, and magnetic properties of one-dimensional chain systems, [W(CN)$_6$(bpy)][Mn(L1)]·0.9H_2O [**1**·0.9H_2O; bpy = 2,2′-bipyridine, L1 = *N*,*N*′-ethylenebis(4-methoxyacetophenylideneiminato) dianion], [W(CN)$_6$(bpy)][Mn(L2)] [**2**; L2 = *N*,*N*′-(1-methylethylene)bis(4-methoxyacetophenylideneiminato) dianion], [W(CN)$_6$(bpy)][Mn(L3)]·0.5H_2O [**3**·0.5H_2O; L3 = *N*,*N*′-(*trans*-1,2-cyclohexanediylethylene)bis(4-methoxysalicylideneiminato) dianion], [W(CN)$_6$(bpy)][Mn(L4)]·2H_2O·0.5CH_3CN [**4**·2H_2O·0.5CH_3CN; L4 = *N*,*N*′-ethylenebis(4-methoxy salicylidineiminato) dianion], and [W(CN)$_6$(bpy)][Mn(L5)]·2H_2O [**5**·2H_2O; L5 = *N*,*N*′-(1-methylethylene)bis(4-methoxysalicylidineiminato) dianion], self-assembled from [W(CN)$_6$(bpy)]$^-$ anions and the corresponding Mn Schiff bases. The central geometry around the W atom is taken into consideration to account for the magnetic behavior. In the distorted square antiprismatic systems, a magnetostructural correlation is established in terms of J and the Mn−N_{ax}−C_{ax} angle in the bridging route.

EXPERIMENTAL SECTION

General Procedures and Materials. All chemicals and solvents used for synthesis were of reagent grade and were used as received. (Ph_4P)[W(CN)$_6$(bpy)] and Mn Schiff bases were synthesized according to the modified literature methods.[29−31]

Li[W(CN)$_6$(bpy)]·0.2MeCN. (Ph_4P)[W(CN)$_6$(bpy)] (100 mg, 0.12 mmol) was dissolved in MeCN (30 mL) and was added to a solution of $LiClO_4$ (13 mg, 0.12 mmol) in MeCN (30 mL). The mixture was stirred for a few minutes. Violet powders precipitated immediately, and were collected by filtration in the dark and air-dried. Yield: 80%. IR (KBr, ν_{CN}): 2146, 2129, and 2116 cm^{-1}. Anal. Calcd for $C_{16.4}H_{8.6}LiN_{8.2}W$: C, 38.53; H, 1.70; N, 22.46. Found: C, 38.89; H, 1.96; N, 22.17.

*[W(CN)$_6$(bpy)][Mn(L1)]·0.9H_2O (**1**·0.9H_2O).* Mn(L1)(H_2O)]ClO_4 (16 mg, 0.030 mmol) in MeCN (10 mL)/H_2O (5 mL) was slowly added to an ethanolic solution (10 mL) of Li[W(CN)$_6$(bpy)]·0.2MeCN (15 mg, 0.030 mmol). The solution was stirred, filtered, and slowly evaporated in the dark, to give deep brown crystals in 24% yield. IR (KBr, ν_{CN}): 2181, 2154, and 2129 cm^{-1}. Anal. Calcd for $C_{36}H_{31.8}N_{10}O_{4.9}MnW$: C, 46.91; H, 3.48; N, 15.20. Found: C, 46.49; H, 3.38; N, 15.36. Compounds **2**−**5** were prepared using the corresponding Mn Schiff bases with L2 to L5 through procedures identical to that for **1**. For **[W(CN)$_6$(bpy)][Mn(L2)]** (**2**), yield: 31%. IR (KBr, ν_{CN}): 2159 and 2129 cm^{-1}. Anal. Calcd for $C_{37}H_{32}N_{10}O_4MnW$: C, 48.33; H, 3.51; N, 15.23. Found: C, 48.38; H, 3.72; N, 15.07. For **[W(CN)$_6$(bpy)][Mn(L3)]·0.5H_2O** (**3**·0.5H_2O), yield: 30%, IR (KBr, ν_{CN}): 2171, 2159, and 2129 cm^{-1}. Anal. Calcd for $C_{38}H_{33}N_{10}O_{4.5}MnW$: C, 48.53; H, 3.54; N, 14.89. Found: C, 48.15; H, 3.65; N, 14.89. For **[W(CN)$_6$(bpy)][Mn(L4)]·2H_2O·0.5CH_3CN** (**4**·2H_2O·0.5CH_3CN), yield: 30%. IR (KBr,

dx.doi.org/10.1021/ic400845z | Inorg. Chem. 2013, 52, 8677−8684

ν_{CN}): 2173, 2164, 2137, and 2132 cm^{-1}. Anal. Calcd for $C_{35}H_{31.5}N_{10.5}O_6MnW$: C, 45.01; H, 3.40; N, 15.75. Found: C, 44.65; H, 3.33; N, 16.10. For $[W(CN)_6(bpy)][Mn(L5)]\cdot 2H_2O$ ($5\cdot 2H_2O$), yield: 28%. IR (KBr, ν_{CN}): 2173, 2163, and 2135 cm^{-1}. Anal. Calcd for $C_{35}H_{31.5}N_{10.5}O_6MnW$: C, 45.70; H, 3.44; N, 15.53. Found: C, 45.32; H, 3.48; N, 15.10.

Physical Measurements. Elemental analyses for C, H, and N were performed at the Elemental Analysis Service Center of Sogang University. Infrared spectra were obtained from KBr pellets with a Bomen MB-104 spectrometer. The magnetic susceptibilities for **1**−**5** were measured with a Quantum Design SQUID (dc) susceptometer. The diamagnetic corrections of **1**−**5** were estimated from Pascal's Tables.

Crystallographic Structure Determination. X-ray data for **1**−**5** were collected on a Bruker SMART APEXII diffractometer equipped with graphite monochromated MoKα radiation (λ = 0.71073 Å). The preliminary orientation matrix and cell parameters were determined from three sets of ϕ scans with different starting angles. Data frames were obtained at scan intervals of 0.5° with an exposure time of 10 s per frame. The reflection data were corrected for Lorentz and polarization factors. Absorption corrections were carried out using SADABS. The structures were solved by direct methods and refined by full-matrix least-squares analysis using anisotropic thermal parameters for most non-hydrogen atoms with the SHELXTL program.[32] Some carbon atoms (C20 for **2** and C1, C2, and C3 for **5**) and the nitrogen atom (N9 for **3**) were isotropically refined because the anisotropic thermal ellipsoids were abnormal. All hydrogen atoms except for those bound to water molecules and isotropically refined atoms were calculated at idealized positions and refined with the riding models. Crystallographic data and the details of data collection are listed in Table 1.

RESULTS AND DISCUSSION

Synthesis and Characterization. The $Li[W(CN)_6(bpy)]$ precursor was prepared through a cation exchange method from the Ph_4P^+ salt. The stoichiometric reaction of $Li[W(CN)_6(bpy)]$ with the corresponding Mn Schiff bases afforded brown crystals of **1**−**5** (Figure 1). The overall structures were

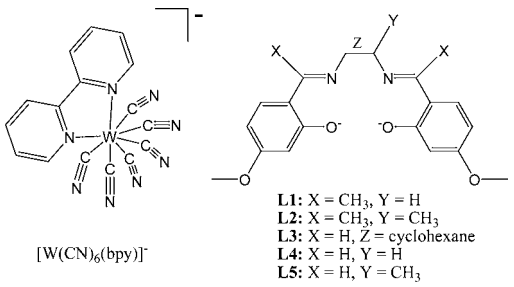

Figure 1. W hexacyanide precursor chelated by bipyridine (left) and the Mn Schiff bases with various substituents (right).

not influenced by the variation in the substituents on the Mn Schiff bases. The characteristic CN stretching modes of the precursor are evident at 2146, 2129, and 2116 cm^{-1} in the IR spectrum. The CN vibrations are centered at 2181, 2154, and 2129 cm^{-1} for **1**, 2159 and 2129 cm^{-1} for **2**, 2171, 2159, and 2129 cm^{-1} for **3**, 2173, 2164, 2137, and 2132 cm^{-1} for **4**, and 2173, 2163, and 2135 cm^{-1} for **5**. Some of the CN absorption bands of **1**−**5** move toward higher frequencies relative to the CN peaks of the precursor, confirming that the cyanides coordinate to the Mn ions.[33]

Description of Structures. Single crystals of all compounds were characterized by means of X-ray crystallography. Compounds **1** and **2** crystallize in the monoclinic crystal system with space group $P2_1/n$, while compounds **3**−**5** crystallize in the orthorhombic system with space group *Pbca* or *Pbcn*. The overall structural patterns of all the complexes are similar despite their different crystal systems.

The crystal structures of **1**−**5** are shown in Figure 2 with the selected atom-labeling schemes. The one-dimensional chain consists of the $W(CN)_6(bpy)^-$ and Mn Schiff base units. Two of the six CN ligands of the precursor bridge neighboring Mn Schiff bases. Each W ion is surrounded by six C atoms from CN groups and two N atoms from bpy. The octacoordinate geometry includes a square antiprism (SAPR, D_{4d}), a dodecahedron (DD, D_{2d}), and a bicapped trigonal prism (BTP, C_{2v}). The precise geometry around the W center was determined by performing continuous shape measures (CShM) analysis.[34,35] The deviation of the central geometry from the reference polyhedral shape was evaluated as tabulated in Table 2. The *S* value obtained from the CShM calculation is zero when the present geometry perfectly matches with the reference polyhedron, and increases as the central geometry deviates from the ideal polyhedron. Therefore, the degree of distortion from the ideal symmetry can be judged from the *S* value. The S_X (X = SAPR, DD, BTP) values compared with the reference symmetry show that the W center in **1** and **2** belongs to a distorted DD, while that in **3**−**5** is assigned to a distorted SAPR. The actual polyhedral shape lies between the interconversion path between SAPR and DD, as manifested by the small Δ value. The W−C distances range from 2.110 to 2.177 Å, and the W−N bond lengths are slightly larger than the W−C distances (2.200−2.243 Å). The W−C−N angles are almost linear, with the smallest angles in the range 168.8−176.1°.

For the Mn^{III} fragments in the one-dimensional chain structures, each Mn atom can be described as a distorted octahedron with a substantial tetragonal elongation. The Mn−N_{ax} (ax = axial) distance in the bridging path is magnetically pertinent. The Mn−N_{ax} bond lengths are 2.370(4) Å for Mn1−N1 and 2.419(4) Å for Mn1a−N6 (**1**; a = 0.5−*x*, −0.5+*y*, 1.5−*z*), 2.439(6) Å for Mn1−N1 and 2.466(5) Å for Mn1b−N6 (**2**; b = 1.5−*x*, −0.5+*y*, 0.5−*z*), 2.345(9) Å for Mn1−N1 and 2.337(12) Å for Mn1c−N6 (**3**; c = 0.5−*x*, 0.5+*y*, *z*), 2.328(10) Å for Mn1−N1 and 2.384(10) Å for Mn1d−N6 (**4**; d = *x*, 2−*y*, 0.5+*z*), and 2.330(16) Å for Mn1−N1 and 2.363(17) Å for Mn1e−N6 (**5**; e = *x*, 2−*y*, 0.5+*z*). The average Mn−$N(O)_{eq}$ (eq = equatorial) distance is around 1.92(7) Å, which is much shorter than the axial distances. These metric parameters verify the existence of the Jahn−Teller effect around the Mn center. Another important internal parameter is the Mn−N_{ax}−C_{ax} angle because it has an impact on magnetic coupling. The related angles are as follows: 176.6(4)° for Mn1−N1−C1 and 161.6(4)° for Mn1a N6−C6 (**1**), 176.4(6)° for Mn1−N1−C1 and 161.4(5)° for Mn1b−N6−C6 (**2**), 167.9(11)° for Mn1−N1−C1 and 167.9(15)° for Mn1c−N6−C6 (**3**), 170.0(9)° for Mn1−N1−C1 and 157.1(11)° for Mn1d−N6−C6 (**4**), and 174.9(17)° for Mn1−N1−C1 and 155.3(16)° for Mn1e−N6−C6 (**5**). The intrachain Mn−W distances are in the range 5.5184−5.7301 Å.

In the crystal packing diagrams (Supporting Information, Figures S1 and S2), the W−Mn chains run along the *b*-axis for **1**−**3** and along the *c*-axis for **4** and **5**. The adjacent chains mingle together via the π−π stacking forces between the benzene rings of the Schiff bases (centroid distance = 3.608 Å for **1**, 3.585 Å for **2**, 3.607 Å for **3**, 3.625 Å for **4**, and 3.724 Å for **5**). The interchain Mn−Mn separations through the noncovalent contacts are equivalent to 9.249 Å for **1**, 9.204 Å

dx.doi.org/10.1021/ic400845z | Inorg. Chem. 2013, 52, 8677−8684

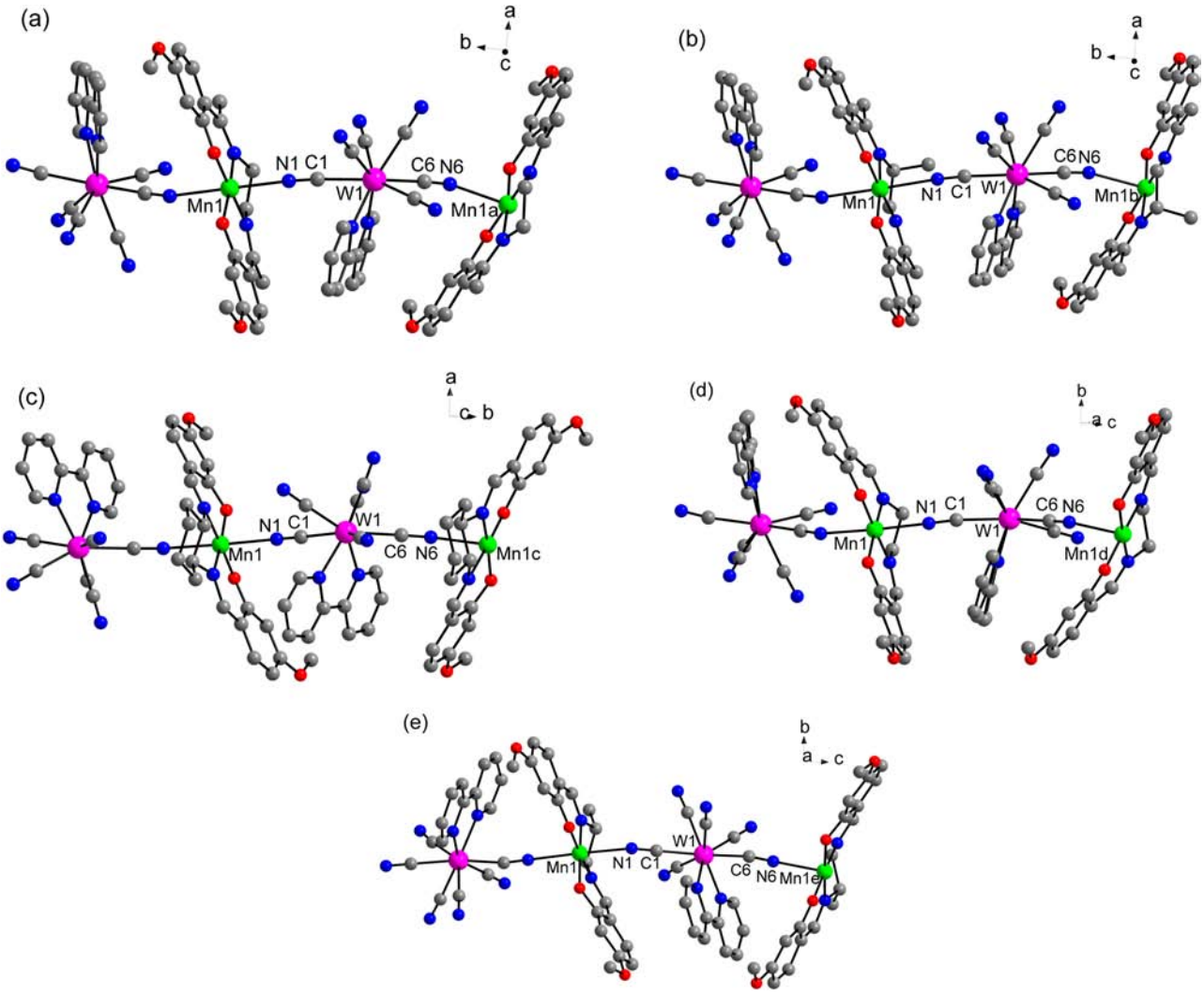

Figure 2. Molecular views of (a) **1**, (b) **2**, (c) **3**, (d) **4**, and (e) **5** with selected atom-labeling schemes. Symmetry codes: a = 0.5−*x*, −0.5+*y*, 1.5−*z*; b = 1.5−*x*, −0.5+*y*, 0.5−*z*; c = 0.5−*x*, 0.5+*y*, *z*; d = *x*, 2−*y*, 0.5+*z*; e = *x*, 2−*y*, 0.5+*z*.

Table 2. Results of the Continuous Shape Measure Analysis[a]

		shape measure (S_x) relative to			Δ	φ	
compds	metal center	SAPR	DD	BTP	(SAPR, DD)	(SAPR > DD)	(DD > SAPR)
1	W1	1.26	0.72	2.19	0.167	66.5%	50.2%
2	W1	1.13	0.78	2.24	0.152	62.8%	52.4%
3	W1	0.67	1.83	2.00	0.283	48.3%	80.0%
4	W1	0.83	1.22	2.30	0.190	53.8%	65.3%
5	W1	0.61	1.52	2.43	0.189	46.1%	72.8%

[a] S_{DD} is the shape measure relative to the dodecahedron, S_{SAPR} the shape measure relative to the square antiprism, S_{BTP} the shape measure relative to the bicapped trigonal prism, Δ(SAPR,DD) indicates the deviation from the DD-SAPR interconversion path, and φ(SAPR > DD) and φ(DD > SAPR) the generalized interconversion coordinates. The sum φ(SAPR > DD) + φ(DD > SAPR) is larger than 100% because of the nonzero value of Δ(SAPR,DD). The parameter Δ is larger than 0.10 which is a threshold value that allows one to describe a given shape as an intermediate between the two ideal shapes.

for **2**, 9.159 Å for **3**, 9.160 Å for **4**, and 9.224 Å for **5**. The shortest interchain distances are found to be 8.539 Å for **1**, 8.652 Å for **2**, 9.105 Å for **3**, 7.420 Å for **4**, and 8.576 Å for **5**.

The spatial conformations were inspected on the basis of the chain skeletons. The Mn Schiff bases in **1** and **2** possess ethylenediamine links arranged in a *-δ-δ-δ-* or *-λ-λ-λ-* discriminative conformational sequence of chelate rings (Supporting Information, Figure S3). In contrast, the linkage in **3**−**5** exhibits a *-δ-λ-δ-* sequence with no helicity in the chain. For **1** and **2**, the *-δ-δ-δ-* and *-λ-λ-λ-*conformations along the chain direction impart a right-handed (P-) and a left-handed (M-) helicity with a long pitch of 20.722 Å (**1**) and 21.188 Å (**2**), respectively (Supporting Information, Figures S4 and S5). Thus, the chiral centers of the Mn Schiff bases facilitate the chain chirality, spreading over the chain through the $[W(CN)_6(bpy)]^-$ moieties. The racemic peculiarity in the chains was also found in several cyanide-based bimetallic systems.[36,37]

Magnetic Properties. In the case of octacyanometallate-based bimetallic systems, it was suggested that the magnetic exchange character is dependent on the geometry around the metal ion.[23] Since the central symmetry of the W atom differs in **1**−**5**, we analyzed the magnetic properties of the chain complexes according to their local environments.

Magnetic Characterizations of 1 and 2 with Distorted Dodecahedral W Geometry. The magnetic susceptibility data for **1** and **2** were collected as a function of temperature at

dx.doi.org/10.1021/ic400845z | Inorg. Chem. 2013, 52, 8677−8684

H = 1000 G (Figure 3a). The $\chi_m T$ values at 300 K for **1** and **2** are 3.41 and 3.51 cm^3 K mol^{-1}, respectively, which are

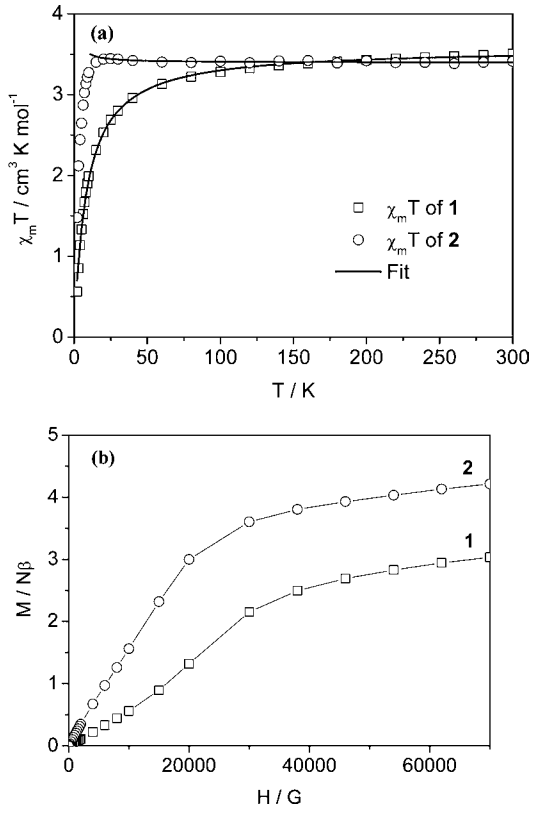

Figure 3. (a) Plots of $\chi_m T$ vs T at 1000 G and (b) magnetization vs H at 2 K for **1** and **2**. The solid lines in panel (a) represent the computed curve, and the solid lines in panel (b) are eye-guides.

consistent with the value (3.38 cm^3 K mol^{-1}) expected from the (S_W, S_{Mn}) = (1/2, 2) spin system assuming g = 2. For **1**, as the temperature decreases, $\chi_m T$ undergoes a slow reduction, followed by a sharp downturn at low temperatures. This implies the operation of typical antiferromagnetic interactions between magnetic spins. The magnetic data for **2** show that $\chi_m T$ slightly increases on cooling, and reaches a maximum of 3.44 cm^3 K mol^{-1} at 20 K. Below the cusp temperature, the $\chi_m T$ product drastically drops. The initial rise in $\chi_m T$ is related to the ferromagnetic couplings between the W^V and Mn^{III} centers within a chain. The sharp drop at low temperatures denotes a combined contribution from interchain antiferromagnetic interactions and/or zero-field splitting.

The magnetic exchange coupling transmitted by cyanide bridges in a chain was examined by using an analytical formula based on the spin Hamiltonian $\mathbf{H} = -2J\Sigma_i(\boldsymbol{S}_{Mn,i}\cdot\boldsymbol{S}_{W,i} + \boldsymbol{S}_{Mn,i}\cdot\boldsymbol{S}_{W,i+1})$, as derived by Seiden.[38,39] The mean-field term (θ) is included as a perturbation of the temperature scale in the fitting process to consider any low-temperature drop of other magnetic contributions. For **1**, fitting the magnetic data to the infinite chain model affords g = 2.05, J = −1.8(2) cm^{-1}, and θ = −6.8 K. The negative J value is ascribed to antiferromagnetic couplings between W^V and Mn^{III} ions mediated by cyanides within a chain. The antiferromagnetic arrangement is assisted by a saturation magnetization of 3.03$N\beta$ at 7 T because the value concurs with the antiferromagnetic consequence of gS = $g(S_{Mn} - S_W)$ = 3$N\beta$ assuming g = 2 (Figure 3b). The same magnetic model was applied to the fit of the magnetic data for **2**. We used the experimental data points at T > 20 K so that interchain antiferromagnetic contributions and zero-field splitting effects were ignored in the fitting process. The best fit gives g = 2.01 and J = 0.4(1) cm^{-1}, which designates the presence of ferromagnetic couplings between spin centers. In the field dependence of the magnetization (M), M amounts to 4.21$N\beta$ at 7 T. The obtained value is much larger than the antiferromagnetic consequence and slightly smaller than the ferromagnetic arrangement (5$N\beta$ assuming g = 2). These results support the intrachain ferromagnetic interactions between W^V and Mn^{III} ions operating via the cyanide bridges. There is no divergence in zero-field-cooled (ZFC) and field-cooled (FC) magnetic data for **1** and **2** (Supporting Information, Figures S6 and S7). In the ac magnetic susceptibility data for **1** and **2**, typical SCM behavior is not observed (Supporting Information, Figures S8 and S9).

Magnetic Characterizations of 3−5 with Distorted Square Antiprismatic Geometry around W. The temperature dependences of the magnetic susceptibilities of **3**−**5** are plotted in Figure 4a. At 300 K, the $\chi_m T$ products for **3**−**5** are

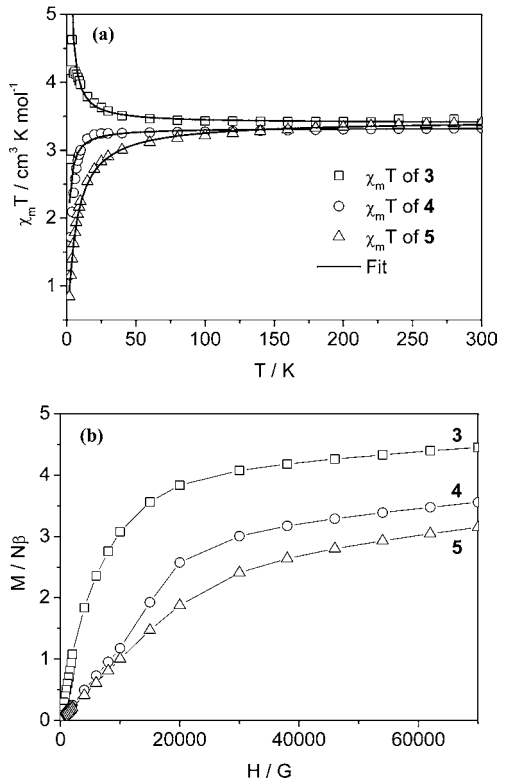

Figure 4. (a) Plots of $\chi_m T$ vs T at 1000 G and (b) magnetization vs H at 2 K for **3**−**5**. The solid lines in panel (a) represent the computed curve, and the solid lines in panel (b) are eye-guides.

equal to 3.41, 3.33, and 3.40 cm^3 K mol^{-1}, respectively, which are in good agreement with the spin-only value calculated from the noncoupled W^V and Mn^{III} spins. The $\chi_m T$ value for **3** increases gradually, and a maximum of 4.63 cm^3 K mol^{-1} is observed at 4 K. This is diagnostic of a ferromagnetic system. A sharp drop is visible below 4 K, probably because of antiferromagnetic interactions and/or zero-field splitting. The magnetic behaviors for **4** and **5** as a function of temperature are analogous, suggesting the operation of overall antiferromagnetic interactions between magnetic centers.

dx.doi.org/10.1021/ic400845z | Inorg. Chem. 2013, 52, 8677−8684

The magnetic coupling constants for **3**−**5** were estimated by utilizing the infinite chain model, as for **1** and **2**. The best fits give parameters of $g = 2.01$ and $J = 1.6(1)$ cm^{-1} for **3**, $g = 1.99$, $J = -0.4(1)$ cm^{-1}, and $\theta = -0.7$ K for **4**, and $g = 2.02$, $J = -1.7(1)$ cm^{-1}, and $\theta = -4.2$ K for **5**. The results unveil that antiferromagnetic couplings are mediated by the cyanide moieties in **4** and **5**, which is opposite to the magnetic character of **3**. In the $M(H)$ data for **3** (Figure 4b), the magnetization value of $4.45N\beta$ is similar to the ferromagnetic result with magnetic anisotropy, which agrees with the expected spin alignment from the $\chi_m T(T)$ curve at $T > 4$ K. The M values at 7 T for **4** and **5** are 3.56 and $3.15N\beta$, respectively, which are closer to the antiferromagnetic arrangement ($3N\beta$) of spins. The M value for **4** is rather large compared with the theoretical value; this disparity may be associated with the spin rotation to the field direction because of weak intrachain magnetic coupling. There is no divergence in zero-field-cooled (ZFC) and field-cooled (FC) magnetic data for **3**−**5** (Supporting Information, Figures S10−S12). The ac magnetic susceptibility data for **3** and **5** show the presence of a long-range antiferromagnetic order at 4.6 and 4.8 K, respectively, which is due to the interchain antiferromagnetic interactions (Supporting Information, Figures S13 and S15). In contrast, the peak feature in the ac data for **4** is not observed (Supporting Information, Figure S14).

Magnetostructural Correlation. To establish a relationship between the structure and magnetic coupling, we examined the important structural and magnetic parameters of **1**−**5**. Density functional theory (DFT) calculations were performed on $[W(CN)_6(bpy)]^-$ to probe the shapes of spin density that govern different types of magnetic exchange couplings. Representative DFT results for **1** and **5** are depicted in Figure 5 and Supporting Information, Figure S16. The spin of W ions is delocalized to the N ends of the cyanide groups in π mode. The π orbitals on the N ends of the bridging cyanide groups can couple with the dσ and dπ orbitals on the adjacent Mn centers in $t_{2g}^3e_g^1$ electronic configuration. The overall magnetic exchange mechanism can be elucidated using the total magnetic coupling constant (J), which in turn can be expressed as a combination of antiferromagnetic (J_{AF}) and ferromagnetic (J_F) terms. In this scheme, J corresponds to $J = (1/n_A n_B)\Sigma_{ij}J_{ij} = J_{AF} + J_F$, where the J_{ij} values are the contributions of pairs of magnetic orbitals, and n is the number of unpaired electrons.[40] In particular, J_{AF} is proportional to the overlap integral between the relevant magnetic orbitals.

Table 3 summarizes the structural parameters and magnetic couplings for one-dimensional W^VMn^{III} bimetallic systems.[30,37,41] Most complexes in SAPR exhibited antiferromagnetic couplings with an exceptional example in the SAPR/DD intermediate geometry showing a ferromagnetic interaction. These data suggest that the magnetic coupling nature is affected by the W geometry. Accordingly, we categorized the systems into DD and SAPR subgroups and inspected each magnetic feature. First, we paid attention to the magnetic properties of **1** and **2** in the shape close to DD geometry. The average Mn−N_{ax}−C_{ax} angles (α) in the bridging pathways are very similar (169.1° for **1** and 168.9° for **2**), while the average Mn−N_{ax} bond length (d) of **1** is shorter than that of **2**. Under these structural circumstances, opposite signs are obtained for the J values (antiferromagnetic in **1** and ferromagnetic in **2**), which signifies that the magnetic behavior should be associated with the difference in bond length. It appears that the elongated distance in **2** weakens the overlap between magnetic orbitals and makes J_F dominate over J_{AF}, eventually leading to the observed ferromagnetic interaction in **2**.

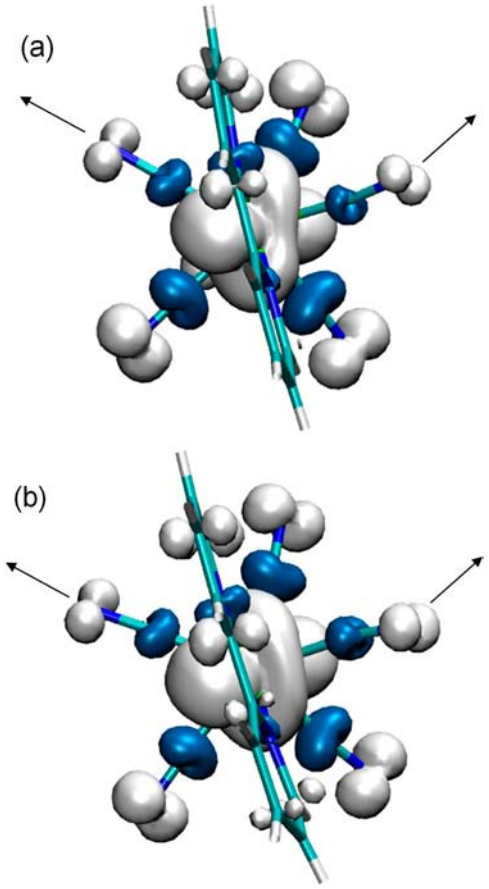

Figure 5. Spin density of the $[W(CN)_6(bpy)]^-$ precursor for (a) **1** and (b) **5**, derived from B3LYP DFT calculations performed with Gaussian 09. The Lanl2dz basis set is taken for the constituent atoms. The arrows indicate the coordination sites to the Mn atoms.

Second, the magnetic properties of several W^VMn^{III} bimetallic systems in the shape close to SAPR were scrutinized in terms of their important structural data as given in Table 3.[12,19,42−44] The Mn−N bond lengths in most complexes are below 2.4 Å, and α changes significantly across the samples. As far as the angle change is concerned, it is evident that J is inclined to increase with increasing angle, and undergoes a crossover from antiferromagnetic to ferromagnetic nature (Figure 6). An expression for the relationship between J and α is derived as J (cm^{-1}) = −151° + 0.91α, and the crossover angle for the change from antiferromagnetic to ferromagnetic coupling is estimated to be around 166°. The proposed relation between J and the Mn−NC angle should be roughly considered. The data from the DD geometry deviate more from the linear line, supporting the conclusion that the central geometry around W and other factors play a role in determining the coupling constant. The dominant magnetic contributions can originate from two types of orbital overlaps: (i) one is between the N pπ orbital of the bridging cyanide and the symmetrically appropriate Mn dπ orbital oriented toward the axial Mn−N_{ax} bond direction, and (ii) the other is between the N pπ orbital and Mn dσ orbital oriented toward the Mn−N_{ax} bond axial direction (Supporting Information, Figure S17). When d is relatively large as in this system with the Jahn−Teller effect, the latter becomes a prime determinant of magnetic

dx.doi.org/10.1021/ic400845z | Inorg. Chem. 2013, 52, 8677−8684

Table 3. Specific Structural Parameters of Selected Bimetallic $W^{V}Mn^{III}$ Complexes and Their Magnetic Natures[a]

complex	ave. Mn−N length (d; Å)	ave. Mn−NC angle (α; deg)	W geometry	J (cm^{-1})	ref
1	2.395	169.1	DD	−1.8(2)	this work
2	2.453	168.9	DD	0.4(1)	this work
3	2.341	167.9	SAPR	1.6(1)	this work
4	2.356	163.6	SAPR	−0.4(1)	this work
5	2.347	165.1	SAPR	−1.7(1)	this work
A	2.328	158.7	SAPR	−4.7(2)	32
B	2.303	159.5	SAPR	−7.6(1)	25
C	2.405	159.9	SAPR	−5.9(1)	25
D	2.378	161.0	SAPR	−6.3(1)	36
E	2.347	157.1	SAPR/DD	0.2(0.1)	32

[a]A = $[W(CN)_6(bpy)][Mn(L6)]\cdot 3MeCN\cdot 3H_2O$ (H_2L6 = *N*,*N*′-bis(2-hydroxynaphthalene-1-carbaldehydene)-1,2-diaminopropane], B = $[W(CN)_6(bpy)][Mn(L7)]\cdot MeCN\cdot MeOH$ [H_2L7 = *N*,*N*′-bis(1′-hydroxy-2′-acetonaphthylidene)-1,2-diaminoethane], C = $[W(CN)_6(bpy)][Mn(L8)]\cdot H_2O$ [H_2L8 = *N*,*N*′-bis(2-hydroxynaphthalene-1-carbaldehydene)-*trans*-diaminocyclohexane], D = $[W(CN)_6(phen)][Mn(L9)]\cdot 0.5MeCN$ [phen =1,10-phenanthroline, H_2L9 = *N*,*N*′-bis(2-hydroxynaphthalene-1-carbaldehydene)-*trans*-diaminocyclohexane], and E = $[W(CN)_6(bpy)][Mn(L10)]\cdot MeCN\cdot H_2O$ (H_2L10 = *N*,*N*′-bis(2-hydroxynaphthalene-1-carbaldehydene)-1,2-diaminoethane]. DD and SAPR indicate distorted shapes closer to the ideal DD and SAPR symmetries, respectively. Hence, the geometry classification should be carefully considered to interpret magnetic coupling.

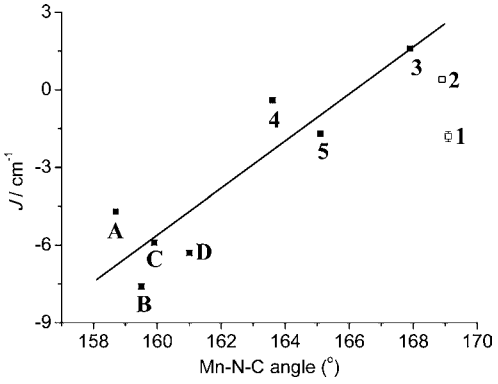

Figure 6. Relationship between magnetic coupling constant (J) and $Mn-N_{ax}-C_{ax}$ angle for the $W^{V}Mn^{III}$ bimetallic systems in a distorted SAPR geometry (filled squares). The data in a distorted DD are shown in open squares.

coupling because this pair of overlap is most effective. That is, the overlap between the N pπ and Mn dσ orbitals gradually lessens as α increases. The progressive reduction in the orbital overlap allows for strict orthogonality of the corresponding orbitals. Consequently, J_{AF} becomes almost negligible relative to J_F leading to ferromagnetic-exchange coupling as shown in **3**. A similar magnetic trend was documented in the $Mn^{III}M^{III}$ (M = Fe, Cr) bimetallic series constructed from Fe cyanides, $[Fe(bpym)(CN)_4]^-$ (bpym = 2,2′-bipyrimidine) and *mer*-$[Fe(L)(CN)_3]^-$ (L = tridentate ligand), and $[Cr(bpy)(CN)_4]^-$ precursor.[21,22,42]

CONCLUSIONS

We have prepared five bimetallic $W^{V}Mn^{III}$ compounds **1**−**5** with one-dimensional chain structures, composed of $[W(CN)_6(bpy)]^-$ anions and $[Mn(Schiff\ base)]^+$ cations. Each W center in **1** and **2** adopts a distorted DD, while that in **3**−**5** displays a distorted SAPR. For the DD geometry, when moving from **1** to **2**, the magnetic nature changes from antiferromagnetic to ferromagnetic as a result of the elongation of the Mn−N_{ax} bond and the consequent predominance of J_F over J_{AF}. On the other hand, for the SAPR geometry, given that the bond lengths are similar, the increase in the $Mn-N_{ax}-C_{ax}$ bond angle is responsible for the variation in J, which is associated with the level of overlap between the N pπ and Mn dσ orbitals. Notably, a magnetostructural correlation is demonstrated for the first time in $W^{V}Mn^{III}$ bimetallic systems based on the $[W(CN)_6(bpy)]^-$ precursor.

ASSOCIATED CONTENT

Supporting Information

X-ray crystallographic files in CIF format, additional structural data for the complexes. This material is available free of charge via the Internet at http://pubs.acs.org.

AUTHOR INFORMATION

Corresponding Author

*E-mail: cshong@korea.ac.kr.

Notes

The authors declare no competing financial interest.

ACKNOWLEDGMENTS

This research was supported by Basic Science Research Program through the National Research Foundation of Korea (NRF) funded by the Ministry of Education, Science and Technology (No. 2012007141), by Priority Research Centers Program (NRF20120005860), and by the Korea CCS R&D Center (KCRC) grant (No. 2012-0008901).

REFERENCES

(1) Cornia, A.; Mannini, M.; Sainctavit, P.; Sessoli, R. *Chem. Soc. Rev.* **2011**, *40*, 3076−3091.
(2) Dechambenoit, P.; Long, J. R. *Chem. Soc. Rev.* **2011**, *40*, 3249−3265.
(3) Sanvito, S. *Chem. Soc. Rev.* **2011**, *40*, 3336−3355.
(4) Sorace, L.; Benelli, C.; Gatteschi, D. *Chem. Soc. Rev.* **2011**, *40*, 3092−3104.
(5) Ferrando-Soria, J.; Serra-Crespo, P.; de Lange, M.; Gascon, J.; Kapteijn, F.; Julve, M.; Cano, J.; Lloret, F.; Pasan, J.; Ruiz-Perez, C.; Journaux, Y.; Pardo, E. *J. Am. Chem. Soc.* **2012**, *134*, 15301−15304.
(6) Roques, N.; Mugnaini, V.; Veciana, J. *Top. Curr. Chem.* **2009**, *293*, 207−258.
(7) Nowicka, B.; Korzeniak, T.; Stefańczyk, O.; Pinkowicz, D.; Chorąży, S.; Podgajny, R.; Sieklucka, B. *Coord. Chem. Rev.* **2012**, *256*, 1946−1971.
(8) Wang, X. Y.; Avendano, C.; Dunbar, K. R. *Chem. Soc. Rev.* **2011**, *40*, 3213−3238.
(9) Alexandru, M. G.; Visinescu, D.; Madalan, A. M.; Lloret, F.; Julve, M.; Andruh, M. *Inorg. Chem.* **2012**, *51*, 4906−4908.
(10) Yoon, J. H.; Kim, H. C.; Hong, C. S. *Inorg. Chem.* **2005**, *44*, 7714−7716.
(11) Yoon, J. H.; Lim, J. H.; Kim, H. C.; Hong, C. S. *Inorg. Chem.* **2006**, *45*, 9613−9615.
(12) Wang, S.; Ding, X.-H.; Zuo, J.-L.; You, X.-Z.; Huang, W. *Coord. Chem. Rev.* **2011**, *255*, 1713−1732.

(13) Peng, Y. H.; Meng, Y. F.; Hu, L.; Li, Q. X.; Li, Y. Z.; Zuo, J. L.; You, X. Z. *Inorg. Chem.* **2010**, *49*, 1905−1912.
(14) Gatteschi, D.; Sessoli, R. *Angew. Chem., Int. Ed.* **2003**, *42*, 268−297.
(15) Sun, H.-L.; Wang, Z.-M.; Gao, S. *Coord. Chem. Rev.* **2010**, *254*, 1081−1100.
(16) Lescouëzec, R.; Toma, L. M.; Vaissermann, J.; Verdaguer, M.; Delgado, F. S.; Ruiz-Pérez, C.; Lloret, F.; Julve, M. *Coord. Chem. Rev.* **2005**, *249*, 2691−2729.
(17) Miyasaka, H.; Saitoh, A.; Abe, S. *Coord. Chem. Rev.* **2007**, *251*, 2622−2664.
(18) Cho, K. J.; Ryu, D. W.; Lim, K. S.; Lee, W. R.; Lee, J. W.; Koh, E. K.; Hong, C. S. *Dalton Trans.* **2013**, *42*, 5796−5804.
(19) Kwak, H. Y.; Ryu, D. W.; Lee, J. W.; Yoon, J. H.; Kim, H. C.; Koh, E. K.; Krinsky, J.; Hong, C. S. *Inorg. Chem.* **2010**, *49*, 4632−4642.
(20) Toma, L.; Lescouezec, R.; Vaissermann, J.; Delgado, F. S.; Ruiz-Perez, C.; Carrasco, R.; Cano, J.; Lloret, F.; Julve, M. *Chem.—Eur. J.* **2004**, *10*, 6130−6145.
(21) Yoo, I. Y.; Ryu, D. W.; Yoon, J. H.; Sohn, A. R.; Lim, K. S.; Cho, B. K.; Koh, E. K.; Hong, C. S. *Dalton Trans.* **2012**, *41*, 1776−1785.
(22) Zhang, Y.-Z.; Gao, S.; Wang, Z.-M.; Su, G.; Sun, H.-L.; Pan, F. *Inorg. Chem.* **2005**, *44*, 4534−4545.
(23) Visinescu, D.; Desplanches, C.; Imaz, I.; Bahers, V.; Pradhan, R.; Villamena, F. A.; Guionneau, P.; Sutter, J.-P. *J. Am. Chem. Soc.* **2006**, *128*, 10202−10212.
(24) Podgajny, R.; Pinkowicz, D.; Korzeniak, T.; Nitek, W.; Rams, M.; Sieklucka, B. *Inorg. Chem.* **2007**, *46*, 10416−10425.
(25) Herrera, J. M.; Marvaud, V.; Verdaguer, M.; Marrot, J.; Kalisz, M.; Mathoniere, C. *Angew. Chem., Int. Ed.* **2004**, *43*, 5468−5471.
(26) Sra, A. K.; Andruh, M.; Kahn, O.; Golhen, S.; Ouahab, L.; Yakhmi, J. V. *Angew. Chem., Int. Ed.* **1999**, *38*, 2606−2609.
(27) Atanasov, M.; Comba, P.; Lampeka, Y. D.; Linti, G.; Malcherek, T.; Miletich, R.; Prikhod'ko, A. I.; Pritzkow, H. *Chem.—Eur. J.* **2006**, *12*, 737−748.
(28) Wang, Y.; Wang, T.-W.; Xiao, H.-P.; Li, Y.-Z.; Song, Y.; You, X.-Z. *Chem.—Eur. J.* **2009**, *15*, 7648−7655.
(29) Szklarzewicz, J. *Inorg. Chim. Acta* **1993**, *205*, 85−89.
(30) Choi, S. W.; Kwak, H. Y.; Yoon, J. H.; Kim, H. C.; Koh, E. K.; Hong, C. S. *Inorg. Chem.* **2008**, *47*, 10214−10216.
(31) Miyasaka, H.; Clérac, R.; Ishii, T.; Chang, H.-C.; Kitagawa, S.; Yamashita, M. *J. Chem. Soc., Dalton Trans.* **2002**, 1528−1534.
(32) Sheldrick, G. M. *SHELXTL*, version 5; Bruker AXS: Madison, WI, 1995.
(33) Kim, J. I.; Kwak, H. Y.; Yoon, J. H.; Ryu, D. W.; Yoo, I. Y.; Yang, N.; Cho, B. K.; Park, J.-G.; Lee, H.; Hong, C. S. *Inorg. Chem.* **2009**, *48*, 2956−2966.
(34) Llunell M.; Casanova D.; Cirera J.; Bofill J. M.; Alemany P.; Alvarez S.; Pinsky M.; Avnir D., *SHAPE*, v1.1b; Barcelona, 2005.
(35) Cirera, J.; Ruiz, E.; Alvarez, S. *Chem.—Eur. J.* **2006**, *12*, 3162−3167.
(36) Yoo, H. S.; Ko, H. H.; Ryu, D. W.; Lee, J. W.; Yoon, J. H.; Lee, W. R.; Kim, H. C.; Koh, E. K.; Hong, C. S. *Inorg. Chem.* **2009**, *48*, 5617−5619.
(37) Choi, S. W.; Ryu, D. W.; Lee, J. W.; Yoon, J. H.; Kim, H. C.; Lee, H.; Cho, B. K.; Hong, C. S. *Inorg. Chem.* **2009**, *48*, 9066−9068.
(38) Harris, T. D.; Bennett, M. V.; Clerac, R.; Long, J. R. *J. Am. Chem. Soc.* **2010**, *132*, 3980−3988.
(39) Seiden, J. *J. Phys., Lett.* **1983**, *44*, 947−952.
(40) Kahn, O. *Molecular Magnetism*; VCH Publishers, Inc.: New York, 1993.
(41) Lee, J.; Lim, K.; Yoon, J.; Ryu, D.; Koo, B.; Koh, E.; Hong, C. *Sci. China Chem.* **2012**, *55*, 1012−1017.
(42) Visinescu, D.; Toma, L. M.; Cano, J.; Fabelo, O.; Ruiz-Perez, C.; Labrador, A.; Lloret, F.; Julve, M. *Dalton Trans.* **2010**, *39*, 5028−5038.
(43) Kim, J. I.; Yoo, H. S.; Koh, E. K.; Kim, H. C.; Hong, C. S. *Inorg. Chem.* **2007**, *46*, 8481−8483.
(44) Przychodzen, P.; Lewiński, K.; Bałanda, M.; Pełka, R.; Rams, M.; Wasiutyński, T.; Guyard-Duhayon, C.; Sieklucka, B. *Inorg. Chem.* **2004**, *43*, 2967−2974.